Journal of Applied Analysis and Computation
Volume 15, Number 5, October 2025, 3185–3206
Website:http://www.jaac-online.com
DOI:10.11948/20240453

A MODULUS ITERATION METHOD FOR NONNEGATIVELY CONSTRAINED PHOTOACOUSTIC IMAGE RECONSTRUCTION

Shuo Wang[1], Li Sun[1] and Yumei Huang[1,†]

Abstract The photoacoustic tomography (PAT) is a new biomedical imaging modality. Its assistance in early clinical diagnosis has become more and more important in the medical field. In the PAT imaging system, when a beam of short-pulsed laser irradiates the biological tissue, the photoacoustic effect results in the generation of the acoustic waves in the tissue. The initial acoustic pressure appearing in the tissue reveals the structures of the tissue. The PAT reconstruction problem aims to obtain the initial acoustic pressure in the tissue from the collected photoacoustic signal informations. In this paper, we propose a nonnegatively constrained PAT reconstruction model regularized by a hybrid Gaussian-Laplacian mixture term. The model can be reformulated as a nonnegatively constrained quadratic programming problem with a positive definite coefficient matrix and it is shown to be equivalent to a linear complementarity problem. We apply a modulus iteration method to solve the linear complementarity problem and its convergence is also demonstrated. Numerical results illustrate that the proposed method is competitive with the existing efficient methods for the PAT reconstruction problem.

Keywords Photoacoustic tomography reconstruction, quadratic programming problem, linear complementarity problem, modulus iteration method.

MSC(2010) 65K15, 90C90, 92C55.

1. Introduction

The photoacoustic tomography (PAT) is a new non-invasive biomedical imaging modality. The PAT can obtain high resolution and high contrast images of deep biological tissue structures in vivo. This technology has a revolutionary impact on clinical medical imaging and it has been widely applied in brain functional imaging, vasculature imaging, breast cancer screening and imaging tumor metastases at the sentinel lymph nodes [34, 37, 39, 56]. The PAT mechanism is based on the photoacoustic effect [10]. When a beam of short-pulsed laser irradiates the biological tissue, the temperature of the tissue rises and the thermal expansion of the tissue happens, which results in the generation of the acoustic waves in the tissue. A set of transducers around the biological tissue surface collect and record these

†The corresponding author.
[1]School of Mathematics and Statistics, Lanzhou University, 730000 Lanzhou, China
Email: 120220907890@lzu.edu.cn(S. Wang), sunli@lzu.edu.cn(L. Sun), huangym@lzu.edu.cn(Y. Huang)

photoacoustic signals. The initial acoustic pressure reveals the structures of the tissue. The purpose of the photoacoustic image reconstruction is to design effective mathematical methods to obtain the initial acoustic pressure in the laser irradiated area by utilizing the collected photoacoustic signal informations. The initial acoustic pressure is proportional to the optical absorption distribution that characterizes the internal structural information of the tissue, so we also can reconstruct the optical absorption distribution. Compared with other medical imaging modalities, such as X-ray computed tomography (CT) and ultrasonic imaging, the PAT allows high spatial resolution and contrast, obtains the images of tissues deep in the biological body, and is free from ionizing radiation. Therefore, the PAT has been playing an important role in the field of medical imaging.

The propagation of the photoacoustic pressure wave is mathematically governed by the following inhomogenous wave equation:

$$\nabla^2 p(\mathbf{r},t) - \frac{1}{c^2}\frac{\partial^2 p(\mathbf{r},t)}{\partial t^2} = -\frac{\beta}{C_p}u(\mathbf{r})\frac{\partial I(t)}{\partial t}, \tag{1.1}$$

where $u(\mathbf{r})$ represents the initial acoustic pressure that we need to determine, $\mathbf{r}$ denotes the tissue position, $p(\mathbf{r},t)$ is the acoustic pressure at the propagation time t, c is the speed of sound transmitted in the tissue medium, C_p is the specific heat, β denotes the thermal expansion coefficient. $I(t)$ is the temporal illumination function. In most cases, $I(t)$ is short enough to be approximated by the Dirac delta function, i.e., $I(t) = \delta(t)$.

By using the Green's function, we get the analytical expression of the acoustic pressure $p(\mathbf{r},t)\,(t \neq 0)$ from the wave equation (1.1) as follows:

$$p(\mathbf{r},t) = \frac{\beta}{4\pi C_p}\frac{\partial}{\partial t}\oiint_{|\mathbf{r}'-\mathbf{r}|=ct}\frac{u(\mathbf{r}')}{t}d\mathbf{r}'. \tag{1.2}$$

Since the acoustic pressure $p(\mathbf{r},t)$ is detected by the transducers and it is known, the back-projection methods [48, 49, 51, 52, 54], the inverse Radon transformation methods [28, 29] have been constructed for the PAT reconstruction and the closed-form analytic inversion formula of the initial acoustic pressure is given. The time reversal methods [25, 42, 53] have also been proposed for the PAT reconstruction. These methods are simple to implement and the computational burden is low. However, in these methods, densely detected photoacoustic signals are required and the reconstructed photoacoustic images suffer from steak-type artifacts and the loss of low-frequency information as well as negative values [11]. In practical applications, due to the limited detection angles of the transducers and the under-sampling data for the purpose of fast data acquisition, the PAT reconstruction problem is an ill-posed inverse problem. Model-based methods can reconstruct the PAT for limited-view and sparse-view photoacoustic signals. In the reconstructed images obtained from the model-based methods, the artifacts caused by the limited-view data and the noises in the photoacoustic signal are removed well.

In the model-based methods, by integrating both sides of equation (1.2) with respect to time t, we have

$$\frac{4\pi C_p t}{\beta}\int_0^t p(\mathbf{r},t)\,dt = \oiint_{|\mathbf{r}'-\mathbf{r}|=ct} u(\mathbf{r}')\,d\mathbf{r}'. \tag{1.3}$$

Based on (1.3), we can see that reconstructing the photoacoustic image u from the collected photoacoustic signal p is an inverse problem. The forward model is

obtained by discretizing (1.3). In the discretization of the right hand side of the equation (1.3), the integral is defined along the arc $|\mathbf{r}' - \mathbf{r}| = ct$, so the discretized points required for the integral computation are located on this arc. We know that u is the reconstructed photoacoustic image, and its discretization values usually need to be determined at rectangular grids. Therefore, in the integral discretization, interpolation methods are often applied to express the values of u located on the arc by the values of u located on the rectangular grids. For example, bilinear interpolation method is used in [12] and circular interpolation method is used in [18]. By considering the discretization errors and noises in the process of the photoacoustic imaging, the discretization result from the above discretized process can be expressed as follows:

$$g = Ru + \eta, \tag{1.4}$$

where $g \in \mathbb{R}^{st}$ is the known photoacoustic signal collected by s transducers, each of which collects the signal at t instants, and $u \in \mathbb{R}^{mn}$ is the photoacoustic image expressed in a vector form. $R \in \mathbb{R}^{st\times mn}$ is the model matrix, which depends only on the speed of sound in the medium and the geometry of the photoacoustic set-up, such as the number and the position of the transducers. Electronic system noise and thermal noise from the transducer are the primary source of noises in the PAT [40]. Therefore, $\eta \in \mathbb{R}^{st}$ is modeled as the additive Gaussian noise with zero mean and standard deviation σ. We focus on the reconstruction of photoacoustic image u from the given photoacoustic signal g.

Reconstructing u from (1.4) is an ill-posed inverse problem. Regularization methods have been proposed for this problem. Shaw et al. [38] and [23] proposed Tikhonov regulariztion models for the PAT reconstruction. Zhang et al. [59] constructed a total variation based model for the sparse-view photoacoustic image reconstruction problem, and the gradient descent algorithm was applied to solve the model. Wang et al. [47] proposed a total variation based model for the PAT reconstruction problem with limited sampling data, and alternating direction method of the multipliers (ADMM) algorithm was applied to solve the model. John et al. [27] and Dong et al. [21] also proposed total variation based models for the PAT reconstruction problem, and the split Bregman algorithm and semismooth Newton scheme were applied to solve the models, respectively. Yalavarthy et al. [55] proposed a total variation constrained model for PAT reconstruction, and a nonlocal means based filtering method was used to improve the effect of reconstruction. Sparsity-based regularization methods have also been proposed for the PAT reconstruction problems. Han et al. [24] proposed a sparsity based reconstruction model for three-dimensional photoacoustic reconstruction and the gradient descent with Barzilai-Borwein linear search algorithm was used to solve the model. Li et al. [30] proposed an photoacoustic tomography image reconstruction model which involved non-local and sparsity regularization terms, and a tailored two-step optimization algorithm was designed to solve the model. In addition, in recent years, some efficient deep learning-based methods [2, 22, 26, 44] have been proposed for PAT reconstruction. Although these methods have improved the results of PAT reconstruction, they still have limitations, such as being time-consuming and demanding a large quantity of data.

In the PAT reconstruction, the pixel values of the photoacoustic images are nonnegative. In most methods for PAT reconstruction, the nonnegative constraint was either completely ignored or simply enforced by setting negative values to zero [50]. Some methods considered the nonnegative constraint. For example, Ding et al. [17]

constructed a nonnegatively constrained PAT reconstruction model and proposed an accelerated projected conjugate gradient algorithm to solve the model; Prakash et al. [36] proposed a PAT reconstruction model based on entropy maximization, where the nonnegative constraint was achieved by adding the relative entropy function of photoacoustic images to the cost function. In [35], a total variation model with pixel value nonnegative constraint was proposed for PAT reconstruction and it was solved by the ADMM algorithm. For the nonnegatively constrained image restoration problem, when the minimization model can be transformed into a linear complementarity problem (LCP), the modulus-based iteration method is an efficient method to solve it. For example, the modulus-based iteration method was applied to solve the nonnegatively constrained Tikhonov, TV and $l_p - l_q$ regularizations models in [6, 58] and [14], respectively.

In this paper, we propose a nonnegatively constrained hybrid Gaussian-Laplacian mixture regularized PAT reconstruction model. By decomposing the image gradient to be the difference of its nonnegative and nonpositive parts, we transform the proposed model into a nonnegatively constrained quadratic programming (NNQP) problem, which can be described as an LCP by utilizing the KKT optimization conditions. We apply an inexact modulus iteration method to effectively solve the LCP and give the theoretical analysis of the proposed method.

The rest of the paper is organized as follows. In Section 2, we give a brief review of the LCP. In Section 3, we propose a nonnegatively constrained hybrid Gaussian-Laplacian mixture regularized PAT reconstruction model and show that this model is equivalent to an LCP. In Section 4, an inexact modulus iteration method is applied to solve the LCP and its convergence analysis is presented. In Section 5, numerical results are given to illustrate the effectiveness of the proposed method. Finally, conclusions are given in Section 6.

2. Linear complementarity problem

The linear complementarity problem LCP (q, A) is described as follows:

$$Az + q \geq 0,\ \ z \geq 0,\ \ z^\top (Az + q) = 0, \tag{2.1}$$

where $z \in \mathbb{R}^n$ is the unknown variable that needs to be determined in LCP (q, A), $A \in \mathbb{R}^{n\times n}$ and $q \in \mathbb{R}^n$ are the known matrix and vector, "$\geq$" represents the component-wise partial ordering between two vectors, $(\cdot)^\top$ denotes the transpose of the corresponding vector or matrix. When A is symmetric positive definite, the LCP (2.1) has a unique solution [15]. The splitting iteration methods have been designed in the literature to obtain the numerical solutions of (2.1). For instance, the projected successive over-relaxation (SOR) iteration method [16], the general fixed-point iteration methods [1, 32, 43], the matrix multisplitting iteration methods [4, 7, 8], and so on. In addition to the splitting iteration methods, modulus iteration methods are efficient methods for solving (2.1). In the modulus iteration methods, the projection of the current iterate onto the first orthant $\{z|z \in \mathbb{R}^n, z \geq 0\}$ is not required in the iteration process. The original modulus iteration method was proposed by Bokhoven in [13]. In recent years, many modified modulus-based iteration methods have been proposed. For example, by introducing a shifting parameter into the modulus iteration methods proposed in [33], Dong and Jiang constructed a new modulus iteration method in [20] for the LCP arising from

nonnegatively constrained least squares problems. In [5], Bai established a class of modulus-based matrix splitting iteration methods by reformulating the LCP as implicit fixed-point equations based on the following theorem.

Theorem 2.1. (see [5]) *Let $A = M - N$ be a splitting of the matrix $A \in \mathbb{R}^{n\times n}$, Ω_1 and Ω_2 be $n \times n$ nonnegative diagonal matrices, Ω and Γ be $n \times n$ positive diagonal matrices such that $\Omega = \Omega_1 + \Omega_2$. For the* LCP (q, A) (2.1), the following statements hold true:

(i) if z is a solution of the LCP (q, A) (2.1), then $x = \frac{1}{2}(\Gamma^{-1}z - \Omega^{-1}(Az + q))$ satisfies the implicit fixed-point equation

$$(M\Gamma + \Omega_1)x = (N\Gamma - \Omega_2)x + (\Omega - A\Gamma)|x| - q; \tag{2.2}$$

(ii) if x is a solution of the implicit fixed-point equation (2.2), then

$$z = \Gamma(|x| + x)$$

is the solution of the LCP (q, A) and $Az + q = \Omega(|x| - x)$.

The modulus-based matrix splitting iteration method to get the solution of the LCP (q, A) (2.1) is given in [5], which contains the detailed splitting iteration method for solving (2.2). We describe it briefly as follows.

Method 2.1. Modulus-Based Matrix Splitting Iteration Method [5]

(1) Give an arbitrary initial vector $x_0 \in \mathbb{R}^n$ and set $k = 0$;

(2) Compute

$$b_k = (N\Gamma - \Omega_2)x_k + (\Omega - A\Gamma)|x_k| - q;$$

(3) Compute x_{k+1} by solving the system of linear equations

$$(M\Gamma + \Omega_1)x = b_k;$$

(4) Set $z_{k+1} = \frac{1}{\gamma}(|x_{k+1}| + x_{k+1})$. If x_{k+1} satisfies the termination criterion, then stop; otherwise, set $k = k + 1$, go to step (2).

In the modulus-based matrix splitting iteration method shown in Method 2.1, the fixed matrices $\Omega_1 = \Omega$ with Ω being a nonnegative diagonal matrix, $\Omega_2 = 0$, $\Gamma = \frac{1}{\gamma}I$ with $\gamma > 0$ and I being the identity matrix are often adopted. Then at each iteration of the modulus-based matrix splitting iteration method, the system of linear equations (2.2) becomes

$$(\Omega + M)x = Nx + (\Omega - A)|x| - \gamma q. \tag{2.3}$$

For the large and sparse LCP defined in (2.1), the problem (2.3) is large and sparse, and iterative methods are often applied to solve it. Iterative methods usually generate an approximate solution with a prescribed accuracy for the linear system. Specifically, in [19], by solving (2.3) using iterative methods, Dong et al. proposed an inexact modulus iteration method for solving the LCP (2.1). The computing process of this inexact modulus iteration method is shown in Method 2.2.

Method 2.2. Inexact Modulus Iteration Method [19, 57]

(1) Give an arbitrary initial vector $x_0 \in \mathbb{R}^n$ and set $k = 0$;

(2) Compute

$$b_k = Nx_k + (\Omega - A)|x_k| - \gamma q, \quad r_k = (\Omega + M)x_k - b_k;$$

(3) Solve the system of linear equations

$$(\Omega + M)y = b_k$$

by a iterative method with the initial guess x_k, such that the approximate solution $\hat{y}$ satisfies

$$(\Omega + M)\hat{y} = b_k + p_k,$$

where

$$\|p_k\| \leq \epsilon_k \|r_k\| \text{ with } \epsilon_k \to 0 \text{ as } k \to \infty;$$

(4) Set $x_{k+1} = \hat{y}$, $z_{k+1} = \frac{1}{\gamma}(|x_{k+1}| + x_{k+1})$. If x_{k+1} satisfies the termination criterion, then stop; otherwise, set $k = k + 1$, go to step (2).

When the matrix A is symmetric positive definite, the convergence of the inexact modulus iteration method was also demonstrated in [19].

3. Proposed model for photoacoustic image reconstruction

Based on (1.4), a regularized model for PAT reconstruction is proposed as follows:

$$\min_{u \geq 0} \frac{1}{2}\|Ru - g\|_2^2 + \frac{\mu}{2}||\nabla u||_2^2 + \beta||\nabla u||_1, \tag{3.1}$$

where $||\cdot||_1$, $||\cdot||_2$ denote the ℓ_1 norm and the Euclidean norm, respectively. $\beta||\nabla u||_1 + \frac{\mu}{2}||\nabla u||_2^2$ is the hybrid Gaussian-Laplacian mixture regularization term [46]. The total variation term $||\nabla u||_1$ can effectively preserve the image edges in the recovered images but the stair-case artifacts often appear. The hybrid Gaussian-Laplacian mixture regularization term can efficiently prevent the stair-case artifacts and preserve the edges in the recovered images. μ and β are the regularization parameters which control the balance among the data-fidelity term $\|Ru - g\|_2^2$ and the two regularization terms $||\nabla u||_2^2$ and $||\nabla u||_1$.

The discrete gradient operator ∇: $\mathbb{R}^{mn\times 1} \to \mathbb{R}^{2mn\times 1}$ is defined by:

$$\nabla u \equiv Du = \begin{pmatrix} D_x u \\ D_y u \end{pmatrix} \tag{3.2}$$

with

$$(D_x u)_{i,j} = \begin{cases} u_{i,j+1} - u_{i,j} & \text{if } j < n, \\ u_{i,1} - u_{i,j} & \text{if } j = n; \end{cases} \quad (D_y u)_{i,j} = \begin{cases} u_{i+1,j} - u_{i,j} & \text{if } i < m, \\ u_{1,j} - u_{i,j} & \text{if } i = m, \end{cases}$$

for $i = 1, 2, \cdots, m, j = 1, 2, \cdots, n$, where $u_{i,j}$ denotes the $((j-1)m + i)$th entry of the vector u. Let

$$v = Du$$

and

$$v^+ = \max(v, 0) \geq 0,\ v^- = \max(-v, 0) \geq 0, \tag{3.3}$$

we can write

$$v = v^+ - v^-.$$

The minimization problem (3.1) can be reformulated as

$$\begin{cases} \min\limits_{u,v^+,v^-} \{\frac{1}{2}\|Ru - g\|_2^2 + \beta(\mathbf{1}^\top v^+ + \mathbf{1}^\top v^-) + \frac{\mu}{2}||v^+ - v^-||_2^2\}, \\ s.t.\ Du = v^+ - v^-, u \geq 0, v^+ \geq 0, v^- \geq 0, \end{cases} \tag{3.4}$$

where $\mathbf{1} \in \mathbb{R}^{2mn\times 1}$ denotes the vector of all ones. By using the penalty method for the constraint $Du = v^+ - v^-$ and the definitions of v^+ and v^- shown in (3.3), the solution of (3.4) can be obtained by solving the following minimization problem:

$$\min_{u,v^+,v^-\geq 0} E(u, v^+, v^-) \tag{3.5}$$

with

$$E(u, v^+, v^-) = \frac{1}{2}\|Ru - g\|_2^2 + \beta(\mathbf{1}^\top v^+ + \mathbf{1}^\top v^-) + \frac{\rho}{2}\|Du - v^+ + v^-\|_2^2 + \frac{\mu}{2}(\|v^+\|_2^2 + \|v^-\|_2^2),$$

where ρ is the penalty parameter. Defining

$$\tilde{g} = [g^\top, 0^\top, 0^\top, 0^\top]^\top,\ \tilde{l} = [0^\top, \mathbf{1}^\top, \mathbf{1}^\top]^\top,$$

and

$$z = [u^\top, {v^+}^\top, {v^-}^\top]^\top,\ q = [-g^\top R, \beta\mathbf{1}^\top, \beta\mathbf{1}^\top]^\top, \tag{3.6}$$

we have

$$\begin{aligned} E(u, v^+, v^-) &= \frac{1}{2} z^\top H^\top H z - \tilde{g}^\top H z + \beta\tilde{l}^\top z + \frac{1}{2}\tilde{g}^\top\tilde{g} \\ &= \frac{1}{2} z^\top W z + q^\top z + \frac{1}{2}\tilde{g}^\top\tilde{g}, \end{aligned}$$

where

$$H = \begin{pmatrix} R & 0 & 0 \\ \sqrt{\rho}D & -\sqrt{\rho}I & \sqrt{\rho}I \\ 0 & \sqrt{\mu}I & 0 \\ 0 & 0 & \sqrt{\mu}I \end{pmatrix}$$

and $I \in \mathbb{R}^{2mn\times 2mn}$ is an identity matrix, as well as

$$W = H^\top H = \begin{pmatrix} R^\top R + \rho D^\top D & -\rho D^\top & \rho D^\top \\ -\rho D & (\rho + \mu)I & -\rho I \\ \rho D & -\rho I & (\rho + \mu)I \end{pmatrix}. \tag{3.7}$$

Therefore, we can reformulate the minimization problem (3.5) as a nonnegatively constrained quadratic programming (NNQP) problem with respect to the variable $z \in \mathbb{R}^{5mn\times 1}$ as follows:

$$\min_{z\geq 0} \frac{1}{2} z^\top W z + q^\top z. \tag{3.8}$$

The following conclusion shows that the matrix W defined in (3.7) is symmetric positive definite under some conditions.

Theorem 3.1. *Let the matrices R be defined in (1.4), D be defined in (3.2) and I be the identity matrix. If $Ker(R) \cap Ker(D) = \{0\}$, then the matrix W defined in (3.7) is symmetric positive definite, where $Ker(\cdot)$ is the kernel or null space of the corresponding matrix.*

Proof. Since $\mu > 0$, $\rho > 0$ and $Ker(R) \cap Ker(D) = \{0\}$, it is obvious that H is a full column rank matrix, so the matrix $W = H^\top H$ is symmetric positive definite. □

Based on the above theorem, the NNQP problem (3.8) is equivalent to a linear complementarity problem LCP (q, W) [6, 60]. We easily obtain the following corollary.

Corollary 3.1. *Let the vectors z and q be defined in (3.6), and the matrix W be defined in (3.7), the NNQP (3.8) resulting from the minimization problem* (3.5) *for the photoacoustic image reconstruction problem is equivalent to the linear complementarity problem LCP (q, W) when $Ker(R) \cap Ker(D) = \{0\}$.*

Therefore, the solution of the minimization problem (3.5) can be obtained by solving the linear complementarity problem LCP (q, W).

4. Modulus iteration method for the proposed model

The linear complementarity problem LCP (q, W) with q being defined in (3.6) and W being defined in (3.7) is solved by the inexact modulus iteration Method 2.2 shown in section 2. In Method 2.2, we set

$$M = W,\ N = 0,\ \Omega = \omega\hat{\Omega},$$

where ω is a positive constant and

$$\hat{\Omega} = \mathrm{diag}(W),$$

$\mathrm{diag}(\cdot)$ denotes the diagonal matrix with the diagonal elements being the diagonal elements of the corresponding matrix. From Theorem 3.1, we know that $\hat{\Omega}$ is positive definite when the condition of the theorem satisfies. The fixed-point equation (2.3) can be expressed as:

$$(\omega\hat{\Omega} + W)x_{k+1} = (\omega\hat{\Omega} - W)|x_k| - \gamma q. \tag{4.1}$$

By utilizing the structure of the matrix W, we can write the diagonal matrix $\hat{\Omega}$ as

$$\hat{\Omega} = \mathrm{diag}(\Omega^1, \Omega^2, \Omega^3) = \mathrm{diag}(\mathrm{diag}(R^\top R + \rho D^\top D), (\rho + \mu)I, (\rho + \mu)I). \tag{4.2}$$

Let

$$P = \begin{pmatrix} I & \frac{\rho}{\rho+\theta}D^\top & -\frac{\rho}{\rho+\theta}D^\top \\ 0 & \frac{\theta}{\theta-\rho}I & \frac{\rho}{\theta-\rho}I \\ 0 & I & I \end{pmatrix},$$

with $\theta = (1+\omega)(\rho+\mu)$. We write

$$x_{k+1} = \begin{pmatrix} x_u^{(k+1)} \\ x_{v^+}^{(k+1)} \\ x_{v^-}^{(k+1)} \end{pmatrix}, \quad b_k = \begin{pmatrix} b_u^{(k)} \\ b_{v^+}^{(k)} \\ b_{v^-}^{(k)} \end{pmatrix} = P(\omega\hat{\Omega} - W)|x_k| - \gamma Pq,$$

where $x_u^{(k+1)}, b_u^{(k)} \in \mathbb{R}^{mn\times 1}$, $x_{v^+}^{(k+1)}, x_{v^-}^{(k+1)}, b_{v^+}^{(k)}, b_{v^-}^{(k)} \in \mathbb{R}^{2mn\times 1}$. By multiplying P on both sides of the fixed-point iteration equation (4.1), we can transform the equation (4.1) into the following system of linear equations

$$\begin{cases} (R^\top R + \zeta D^\top D + \omega\Omega^1)x_u^{(k+1)} = b_u^{(k)}, \\ x_{v^+}^{(k+1)} = \dfrac{1}{\rho+\theta}(\rho D x_u^{(k+1)} + b_{v^+}^{(k)}), \\ x_{v^-}^{(k+1)} = -x_{v^+}^{(k+1)} + \dfrac{1}{\theta-\rho} b_{v^-}^{(k)}, \end{cases} \tag{4.3}$$

where $\zeta = \rho(\theta-\rho)/(\theta+\rho) > 0$, and the matrix Ω^1 is symmetric positive definite when $Ker(R) \cap Ker(D) = \{0\}$. For the first linear system in (4.3), the preconditioned conjugate gradient method combined with the preconditioning matrix $K = \mathrm{diag}(R^\top R) + \zeta D^\top D + \omega\Omega^1$ is applied to solve it. The incomplete LU decomposition is used in the computation. Once $x_u^{(k+1)}$ is known, $x_{v^+}^{(k+1)}, x_{v^-}^{(k+1)}$ can be calculated straightforwardly from the second and the third formulae in (4.3), respectively.

The inexact modulus iteration method for solving LCP (q, W) with W and q being defined in (3.7) and (3.6) is described in Algorithm 1. The convergence of Algorithm 1 is also shown in the following theorem.

Theorem 4.1. *Let ω and γ be positive constants shown in Algorithm 1. Suppose $Ker(R)\cap Ker(D) = \{0\}$ and the condition (4.12) holds. Then for any initial vector $x_0 \in \mathbb{R}^{5mn\times 1}$, the iterative sequence $\{z_k\}_{k=0}^{\infty}$ generated by Algorithm 1 converges to the unique solution z_* of LCP (q, W) which is equivalent to the photoacoustic image reconstruction problem (3.5), where q is defined in (3.6) and W is defined in (3.7).*

Proof. Let ω and γ be positive constants in Algorithm 1. Since the matrix W defined in (3.7) is symmetric positive definite, by utilizing Corollary 2 in [6], we know that LCP (q, W) has a unique solution z_*. Let $\hat{\Omega}$ be the diagonal matrix defined in (4.2). From Theorem 2.1, $x_* = \frac{1}{2}(\frac{1}{\gamma}z_* - (\omega\hat{\Omega})^{-1}(Wz_* + q))$ is the solution of the following implicit fixed-point equation

$$P(\omega\hat{\Omega} + W)x = P(\omega\hat{\Omega} - W)|x| - \gamma Pq. \tag{4.4}$$

Given an initial vector $x_0 \in \mathbb{R}^{5mn\times 1}$, after k iteration steps of

$$P(\omega\hat{\Omega} + W)x_{k+1} = P(\omega\hat{\Omega} - W)|x_k| - \gamma Pq + p_k, \tag{4.5}$$

a sequence of the inexact solutions $x_{k+1}(k = 0, 1, 2, \cdots)$ of (4.4) is generated by Algorithm 1. We represent $x_k = [(x_u^{(k)})^\top, (x_{v^+}^{(k)})^\top, (x_{v^-}^{(k)})^\top]^\top$ with $x_u^{(k)} \in \mathbb{R}^{mn\times 1}$, $x_{v^+}^{(k)}$, $x_{v^-}^{(k)} \in \mathbb{R}^{2mn\times 1}$. By making use of the special structure of the coefficient matrix $P(\omega\hat{\Omega} + W)$ shown in (4.3), we can obtain the solution x_{k+1} of (4.5) by

solving $x_u^{(k+1)}$, $x_{v^+}^{(k+1)}$ and $x_{v^-}^{(k+1)}$ separately. According to the computing process shown in Algorithm 1, $x_u^{(k+1)}$ can be obtained by solving the first linear system in (4.3) using the preconditioned conjugate gradient method and $x_{v^+}^{(k+1)}, x_{v^-}^{(k+1)}$ can be directly obtained by using the second and third formulae in (4.3). From (4.11) and (4.13), we have $p_k = [(p_u^{(k)})^\top, 0^\top, 0^\top]^\top$, where $p_u^{(k)}$ is considered as a perturbation of $b_u^{(k)}$ in (4.11). Suppose x_* is the exact solution of (4.4), for $k = 0, 1, 2, \cdots$, we obtain

$$x_{k+1} - x_* = (\omega\hat{\Omega} + W)^{-1}(\omega\hat{\Omega} - W)(|x_k| - |x_*|) + (\omega\hat{\Omega} + W)^{-1}P^{-1}p_k. \tag{4.6}$$

Assume that $p_u^{(k)}$ satisfies $\|p_u^{(k)}\|_2 \le \epsilon_k \|r_k\|_2$ with $\epsilon_k \to 0$ as $k \to \infty$, where r_k is defined in (4.10). We have

$$\|p_k\|_2 = \|p_u^{(k)}\|_2 \le \epsilon_k \|r_k\|_2 \ \text{ with } \epsilon_k \to 0 \text{ as } k \to \infty.$$

We can get the norm bound of (4.6) as

$$\begin{aligned}
&\|x_{k+1} - x_*\|_2 \\
=&\|(\omega\hat{\Omega} + W)^{-1}(\omega\hat{\Omega} - W)(|x_k| - |x_*|) + (\omega\hat{\Omega} + W)^{-1}P^{-1}p_k\|_2 \\
\le&\|(\omega\hat{\Omega} + W)^{-1}(\omega\hat{\Omega} - W)\|_2\|x_k - x_*\|_2 + \epsilon_k\|(\omega\hat{\Omega} + W)^{-1}P^{-1}\|_2\|r_k\|_2 \\
\le&\|(I + (\omega\hat{\Omega})^{-1/2}W(\omega\hat{\Omega})^{-1/2})^{-1}(I - (\omega\hat{\Omega})^{-1/2}W(\omega\hat{\Omega})^{-1/2})\|_2\|x_k - x_*\|_2 \\
&+ \epsilon_k\|(\omega\hat{\Omega} + W)^{-1}P^{-1}\|_2(\|P(\omega\hat{\Omega} + W)\|_2 + \|P(\omega\hat{\Omega} - W)\|_2)\|x_k - x_*\|_2 \\
\le&L_k\|x_k - x_*\|_2,
\end{aligned} \tag{4.7}$$

where

$$L_k = \epsilon_k\delta + \mu \tag{4.8}$$

with

$$\begin{aligned}
\delta &\equiv \|(\omega\hat{\Omega} + W)^{-1}\|_2\|P^{-1}\|_2\|P\|_2(\|\omega\hat{\Omega} + W\|_2 + \|\omega\hat{\Omega} - W\|_2), \\
\mu &\equiv \|(I + (\omega\hat{\Omega})^{-1/2}W(\omega\hat{\Omega})^{-1/2})^{-1}(I - (\omega\hat{\Omega})^{-1/2}W(\omega\hat{\Omega})^{-1/2})\|_2.
\end{aligned}$$

As the matrix W is symmetric positive definite, and the matrix $(\omega\hat{\Omega})^{-1/2}$ is a positive definite diagonal matrix, the matrix $(\omega\hat{\Omega})^{-1/2}W(\omega\hat{\Omega})^{-1/2}$ is symmetric positive definite. Therefore, it holds that

$$\mu = \max_{\lambda \in \sigma((\omega\hat{\Omega})^{-1/2}W(\omega\hat{\Omega})^{-1/2})} \left|\frac{1-\lambda}{1+\lambda}\right| < 1,$$

where $\sigma((\omega\hat{\Omega})^{-1/2}W(\omega\hat{\Omega})^{-1/2})$ denotes the set of eigenvalues of $(\omega\hat{\Omega})^{-1/2}W \times (\omega\hat{\Omega})^{-1/2}$; see [9]. Since $\lim\limits_{k\to\infty} \epsilon_k = 0$, there is an integer k_0 such that for all $k \ge k_0 \ge 1$,

$$\epsilon_k\delta < \frac{1-\mu}{2}. \tag{4.9}$$

According to (4.7), (4.8) and (4.9), we have

$$L_k < \theta := \frac{1+\mu}{2} < 1,$$

and for $k \geq k_0$,

$$\|x_{k+1} - x_*\|_2 \leq \theta^{k+1-k_0} \|x_0 - x_*\|_2 \prod_{i=0}^{k_0-1} L_i \to 0, \text{ as } k \to \infty.$$

By utilizing the result z_k shown in (4.14) in Algorithm 1, we easily have

$$z_k \to z_*, \text{ as } k \to \infty,$$

for any initial vector $x_0 \in \mathbb{R}^{5mn \times 1}$. □

5. Numerical experiments

In this section, we present numerical results to illustrate the performance and effectiveness of the proposed method for the PAT reconstruction problem. Images "Simulation" which is a simulated phantom, "Breast" which is a breast phantom [31] and "Tumor" which is a mouse brain phantom [3] are used in the experiments. They are both with size 100×100 and shown in Figure 1. We synthetically get the photoacoustic pressure signals g in (1.4). The system matrix R in (1.4) is obtained by using the method proposed in [59]. In the experiment, the speed of sound is taken as 1500 m/s. 60 detectors are placed equidistantly on a circle that surrounds the imaging tissue and each detector records information at 60 instants with equal time intervals. Therefore, the size of the system matrix R is 3600×10000. The white Gaussian noise with the standard deviations $\sigma = 10$ and $\sigma = 20$ are used in the experiments for each image. The methods "ADMMTV+" proposed in [35] and "SBTV-l2" proposed in [27] for the PAT reconstruction are utilized for all the reconstruction tests in the experiments for the purpose of comparisons. Two measures peak signal-to-noise ratio (PSNR) and structural similarity (SSIM) [41, 45] are applied for judging the reconstruction quality. In the experiment, we find that if β is too large, the reconstructed PAT images are oversmooth, if β is too small, there are residue noises in the reconstructed PAT images. And $\beta = 2$ is the best for getting desirable reconstructed images. Small parameter μ is good and we set it to be 0.005. When parameter ρ is located in the interval $[0.1, 1]$, the reconstructed results are fine. For parameter ω, we find that if it is too small, the consumed time is longer, and $\omega = 0.2$ is best for both the consumed time and reconstructed effect. For parameter γ, we find that if it is set as the value in the interval $[1, 3]$, the reconstructed results are better. In the final experiment, the parameters are set as $\mu = 0.005$, $\omega = 0.2$, $\gamma = 2$, $\rho = 0.2$, $\beta = 2$ respectively. Such parameters can get the best reconstruction results. The stopping criteria parameters are set as $\epsilon = 5 \times 10^{-3}$ and $\epsilon_k = 1/k^2$ with k being the outer iteration step in Algorithm 1. The parameters in each compared method are selected to be those which make the reconstructed PSNRs and SSIMs best in the experiments. All the computations are performed using Matlab R2018a, on a personal computer with 3.00GHz CPU and 8 GB RAM.

The numerical results of the experiments obtained by the proposed method and the compared methods are shown in Table 1 and Table 2, where "CPU" represents the computing time in seconds, and the best "CPU", "PSNR" and "SSIM" are shown in boldface. From these tables, we can see that the computing time consumed in "MODULUS" method is less than that required in the compared methods for each experiment. We can also see that "PSNR" and "SSIM" obtained by

Algorithm 1 Modulus Iteration Method for Photoacoustic Image Reconstruction

1 Set the positive valued of the constants ω, γ and the tolerances ϵ, ϵ_k, Let $\hat{\Omega}$ and Ω^1 be the diagonal matrices defined in (4.2). Give an initial guess x_0, we have $z_0 = \frac{1}{\gamma}(|x_0| + x_0)$, use k be the iteration index, and set $k = 0$;

2 Compute

$$b_k = P(\omega\hat{\Omega} - W)|x_k| - \gamma Pq, \quad r_k = b_k - P(\omega\hat{\Omega} + W)x_k, \tag{4.10}$$

where $b_k = [(b_u^{(k)})^\top, (b_{v^+}^{(k)})^\top, (b_{v^-}^{(k)})^\top]^\top$. Correspondingly, $x_k = [(x_u^{(k)})^\top, (x_{v^+}^{(k)})^\top, (x_{v^-}^{(k)})^\top]^\top$;

3 Using $x_u^{(k)}$ as the initial guess, the preconditioned conjugate gradient method with the preconditioner $K = \mathrm{diag}(R^\top R) + \zeta D^\top D + \omega\Omega^1$ is applied to solve the system of linear equations

$$(R^\top R + \zeta D^\top D + \omega\Omega^1)y = b_u^{(k)},$$

such that the approximate solution $\hat{y}$ satisfies

$$(R^\top R + \zeta D^\top D + \omega\Omega^1)\hat{y} = b_u^{(k)} + p_u^{(k)}, \tag{4.11}$$

where

$$\|p_u^{(k)}\|_2 \le \epsilon_k \|r_k\|_2 \text{ with } \epsilon_k \to 0 \text{ as } k \to \infty. \tag{4.12}$$

We get $x_u^{(k+1)} = \hat{y}$ and

$$\begin{aligned} x_{v^+}^{(k+1)} &= \frac{1}{\rho + \theta}(\rho D x_u^{(k+1)} + b_{v^+}^{(k)}), \\ x_{v^-}^{(k+1)} &= -x_{v^+}^{(k+1)} + \frac{1}{\theta - \rho} b_{v^-}^{(k)}. \end{aligned} \tag{4.13}$$

4 Calculate

$$z_{k+1} = \frac{1}{\gamma}(|x_{k+1}| + x_{k+1}). \tag{4.14}$$

Denote

$$\mathrm{Re} = \frac{\|\mathrm{z_{k+1}} - \mathrm{z_k}\|_2}{\|\mathrm{z_k}\|_2}. \tag{4.15}$$

If $\mathrm{Re} < \epsilon$, break; otherwise set $k = k + 1$, go to step 2.
Output $z = z_{k+1}$.

"MODULUS" method are the best in each experiment. For example, for the image "Tumor", when $\sigma = 10$, the "PSNR" obtained by the "MODULUS" method is 5.33 larger than that obtained by "SBTV-l2" method and 0.61 larger than that obtained by "ADMMTV+" method; and the "SSIM" obtained by "MODULUS" method are 0.077 larger than that got by "SBTV-l2" method and 0.0068 larger than that got by "ADMMTV+" method, which all indicate that the proposed "MODULUS" method is more efficient than the compared methods. We also notice that the difference of

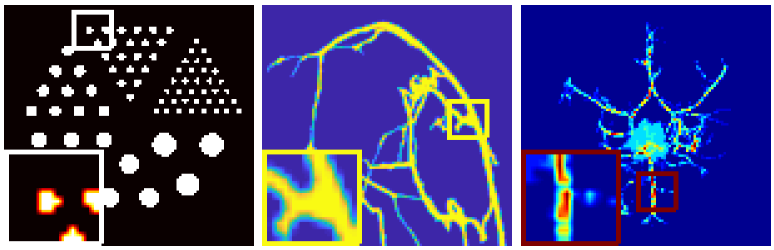

Figure 1. The "Simulation" (left), "Breast" (middle) and "Tumor" (right) phantoms.

Table 1. Numerical results of the experiments when $\sigma = 10$.

Method	Measure	Image		
		Simulation	Breast	Tumor
SBTV-l2	CPU	4.88	5.21	8.13
	PSNR	36.30	22.76	28.52
	SSIM	0.9894	0.9043	0.9038
ADMMTV+	CPU	4.68	5.07	6.46
	PSNR	38.46	29.89	33.24
	SSIM	0.9973	0.9894	0.9740
MODULUS	CPU	**3.25**	**3.57**	**4.17**
	PSNR	**38.99**	**30.41**	**33.85**
	SSIM	**0.9992**	**0.9925**	**0.9808**

Table 2. Numerical results of the experiments when $\sigma = 20$.

Method	Measure	Image		
		Simulation	Breast	Tumor
SBTV-l2	CPU	4.13	4.60	6.56
	PSNR	30.80	22.26	28.04
	SSIM	0.9735	0.8915	0.8837
ADMMTV+	CPU	4.38	4.33	4.88
	PSNR	34.07	27.62	31.27
	SSIM	0.9866	0.9811	0.9532
MODULUS	CPU	**3.09**	**3.70**	**4.03**
	PSNR	**34.55**	**28.64**	**32.02**
	SSIM	**0.9960**	**0.9875**	**0.9661**

the results between the "MODULUS" method and the "ADMMTV+" method is not big. Since the nonnegative constraint of the PAT images is taken into account in both the "MODULUS" and "ADMMTV+" methods, we conclude that the consideration of the nonnegative constraint in the construction of the PAT reconstruction model is very important for the high quality of the reconstructed PAT images.

In Figure 2, we show the reconstructed "Simulation" images when the corresponding photoacoustic signals are contaminated by Gaussian noises with $\sigma = 10$

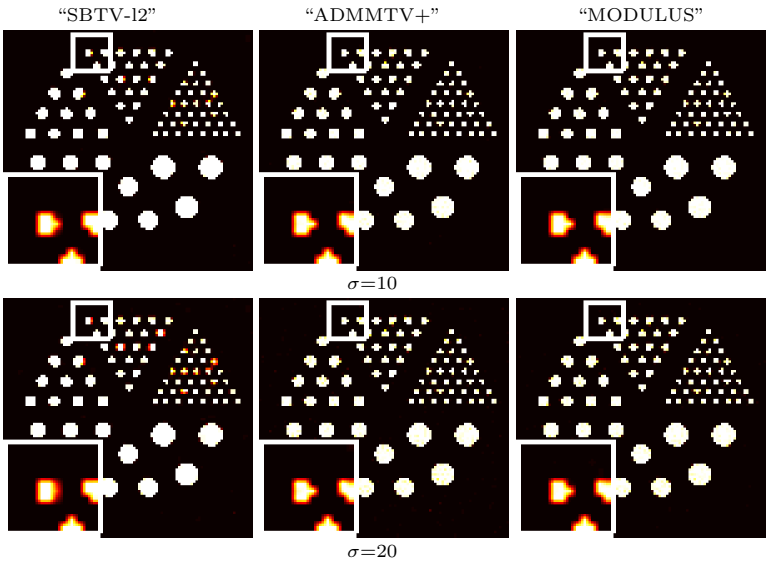

Figure 2. Experimental results for "Simulation" image. From the first to the second line, reconstructed images for noise levels: $\sigma = 10, 20$, respectively; From the first to the third column, reconstructed images by: "SBTV-L2", "ADMMTV+" and "MODULUS", respectively.

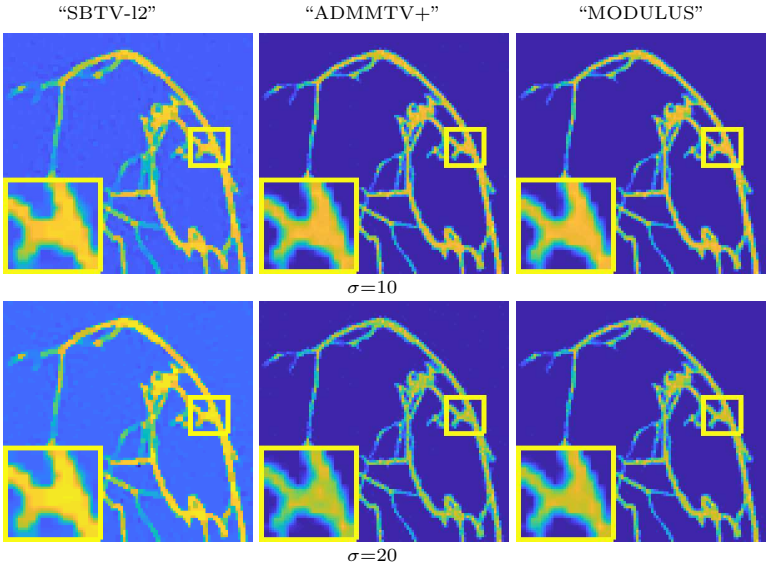

Figure 3. Experimental results for "Breast" image. From the first to the second line, reconstructed images for noise levels: $\sigma = 10, 20$, respectively; From the first to the third column, reconstructed images by: "SBTV-L2", "ADMMTV+" and "MODULUS", respectively.

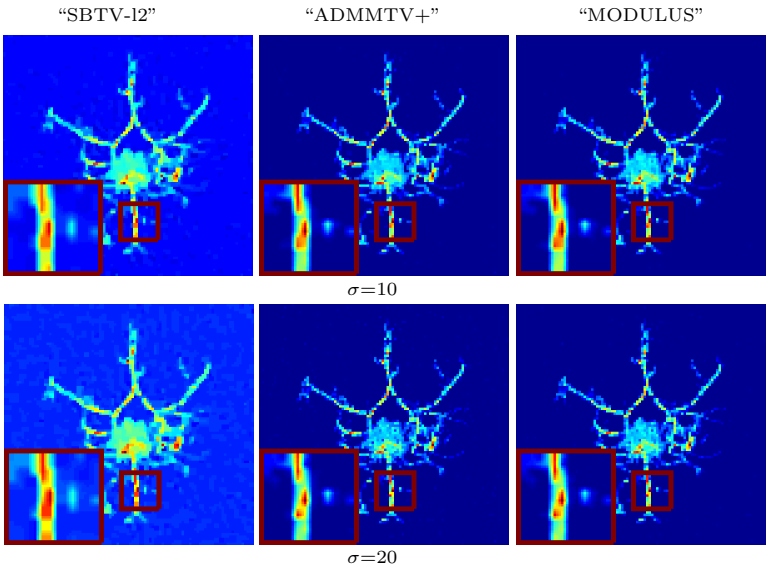

Figure 4. Experimental results for "Tumor" image. From the first to the second line, reconstructed images for noise levels: $\sigma = 10, 20$, respectively; From the first to the third column, reconstructed images by: "SBTV-L2", "ADMMTV+" and "MODULUS", respectively.

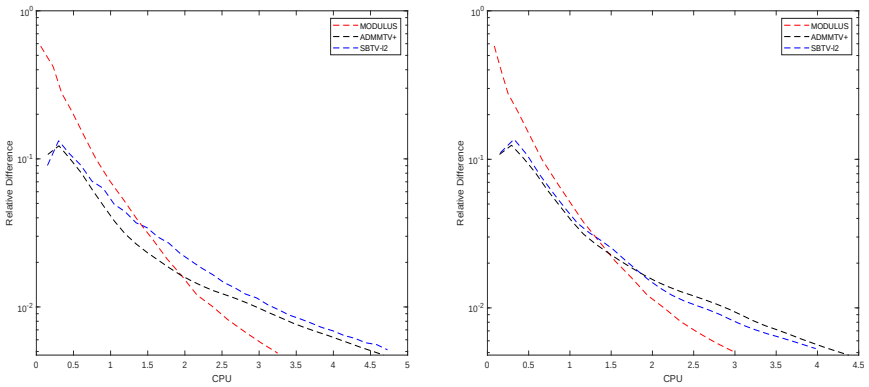

Figure 5. "Re" versus "CPU" for "Simulation", when (a) $\sigma = 10$; (b) $\sigma = 20$.

and $\sigma = 20$. The reconstructed "Simulation" images obtained by "SBTV-l2", "ADMMTV+" and "MODULUS" methods are shown from the first column to the third column respectively. In order to assess the reconstructed visual effects more clearly, for every reconstructed image, we extract one small block encircled by white square box and show it in the lower left corner of the image within a larger white square box for the sake of saving space. Whether from the whole reconstructed image or the enlarged square block, we can see that the edges are sharper in the reconstructed images obtained by "MODULUS" method than in those obtained by

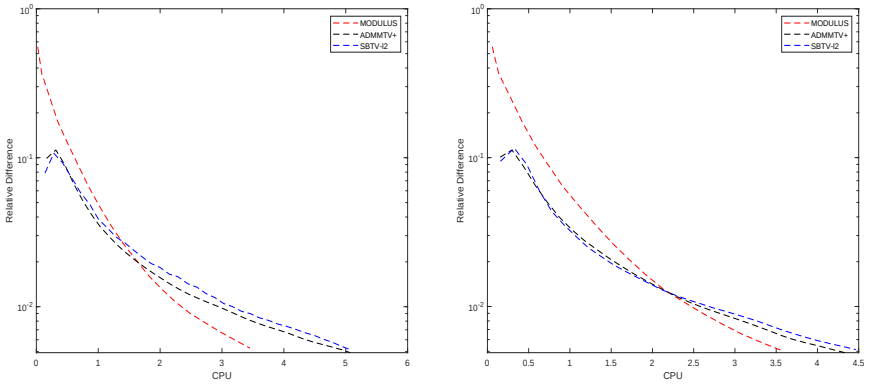

(a) (b)

Figure 6. "Re" versus "CPU" for "Breast", when (a) $\sigma = 10$; (b) $\sigma = 20$.

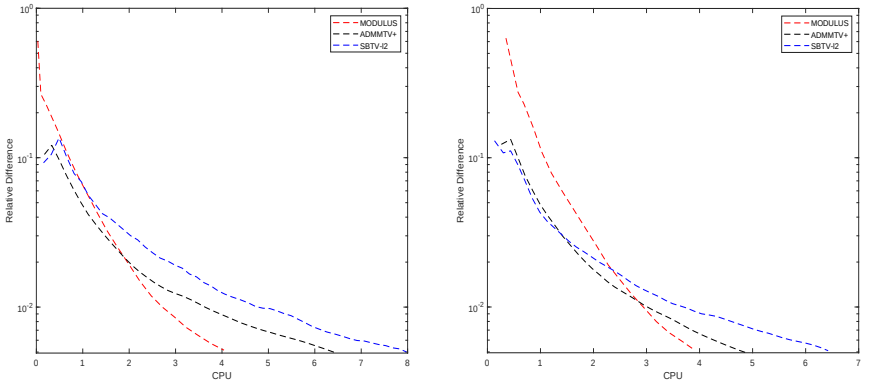

(a) (b)

Figure 7. "Re" versus "CPU" for "Tumor", when (a) $\sigma = 10$; (b) $\sigma = 20$.

"ADMMTV+" and "SBTV-l2" methods. In Figure 3, we show the reconstructed "Breast" images when the corresponding photoacoustic signals are contaminated by Gaussian noises with $\sigma = 10$ and $\sigma = 20$. The images shown from the first column to the third column are reconstructed "Breast" images utilizing "SBTV-l2", "ADMMTV+" and "MODULUS" methods respectively. For every reconstructed image, we extract one small block encircled by yellow square box and show it in the lower left corner of the image within a larger yellow square box. From these figures, we can see that whether from the whole reconstructed image or the enlarged square block, the background of the reconstructed "Breast" image is smoother and the edges of the pale blue parts are sharper in the reconstructed images obtained by "MODULUS" method than in those obtained by "ADMMTV+" and "SBTV-l2" methods, especially for larger noise level $\sigma = 20$. We note that the difference in the visual effects of the reconstructed images between the "MODULUS" method and

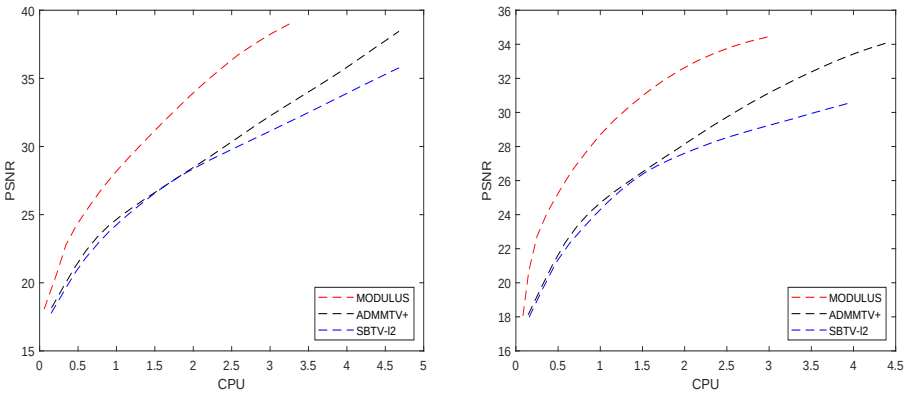

Figure 8. "PSNR" versus "CPU" for 'Simulation", when (a) $\sigma = 10$; (b) $\sigma = 20$.

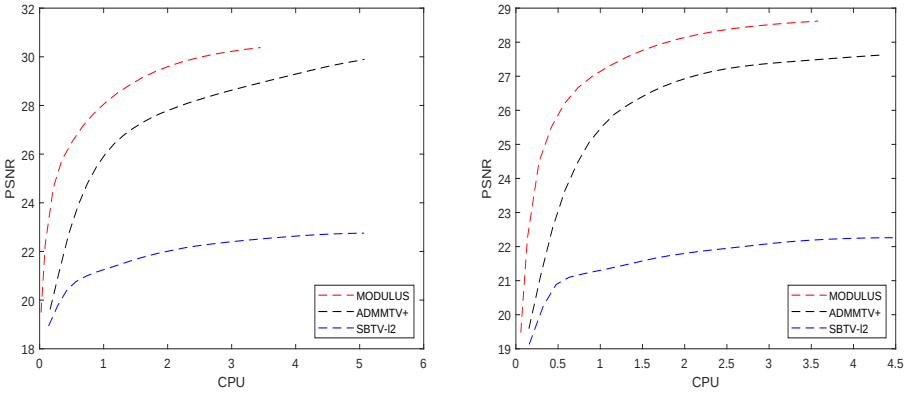

Figure 9. "PSNR" versus "CPU" for "Breast", when (a) $\sigma = 10$; (b) $\sigma = 20$.

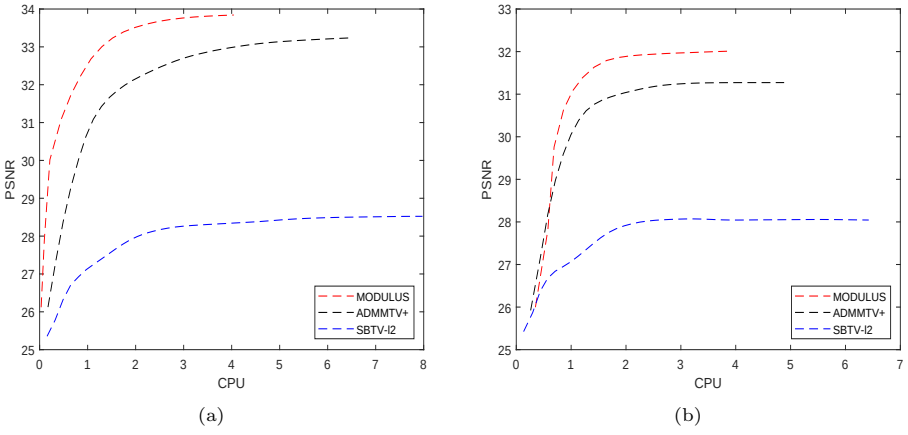

Figure 10. "PSNR" versus "CPU" for "Tumor", when (a) $\sigma = 10$; (b) $\sigma = 20$.

the "ADMMTV+" method is not big. Figure 4 shows the reconstructed "Tumor" images when the corresponding photoacoustic signals are contaminated by Gaussian noises with $\sigma = 10$ and $\sigma = 20$ respectively. The reconstructed "Tumor" images obtained by "SBTV-l2", "ADMMTV+" and "MODULUS" methods are shown from the first column to the third column, respectively. For each image in Figure 4, we also extract one small block encircled by a red square box and show it in the lower left corner of the image within a larger red square box. From these figures, we can see that the background of the reconstructed "Tumor" image is smoother in the reconstructed images obtained by "MODULUS" method than in those obtained by "ADMMTV+" and "SBTV-l2" methods. We also note that the difference in the visual effects of the reconstructed images between the "MODULUS" method and the "ADMMTV+" method is not big. The visual qualities are consistent with the quantative results of reconstructed images shown in Table 1 and Table 2.

In Figures 5-7, we plot curves of the relative difference "Re" given in (4.15) in Algorithm 1 versus "CPU" time for the six experiments. The figures show that the convergence rate of the proposed "MODULUS" method is the fastest. In Figures 8-10, we plot curves of the "PSNR" versus "CPU" time for the six experiments. From these figures, we observe that the proposed "MODULUS" method can converge to a higher "PSNR" faster than the "SBTV-l2" and "ADMMTV+" methods, which is in accordance with the quantative results of the reconstructed images presented in Table 1 and Table 2. From the convergence curves and numerical results, we can conclude that the "MODULUS" method performs better in terms of the reconstructed quality and computational efficiency.

6. Conclusions

In this paper, we propose a hybrid Gaussian-Laplacian mixture regularization model for the PAT reconstruction. We formulate this problem as a nonnegatively constrained quadratic programming problem, which is equivalent to a linear complementarity problem. The modulus iteration method is applied to solve this linear complementarity problem. Experimental results demonstrate the stability and efficiency of the proposed method for the PAT reconstruction problem in terms of both the reconstructed quality of the PAT and computational efficiency.

Acknowledgements

The authors are grateful to the anonymous referees for their useful comments and suggestions.

References

[1] B. H. Ahn, *Solution of nonsymmetric linear complementarity problems by iterative methods*, J. Optim. Theory Appl., 1981, 33(2), 175–185.

[2] S. Antholzer, M. Haltmeier and J. Schwab, *Deep learning for photoacoustic tomography from sparse data*, Inverse Probl. Sci. Eng., 2019, 27(7), 987–1005.

[3] S. Arridge, P. Beard and M. Betcke, *Accelerated high-resolution photoacoustic tomography via compressed sensing*, Phys. Med. Biol., 2016, 61(24), 8908.

[4] Z. Bai, *On the convergence of the multisplitting methods for the linear complementarity problem*, SIAM J. Matrix Anal. Appl., 1999, 21(1), 67–78.

[5] Z. Bai, *Modulus-based matrix splitting iteration methods for linear complementarity problems*, Numer. Linear Algebra Appl., 2010, 17(6), 917–933.

[6] Z. Bai, A. Buccini, K. Hayami, L. Reichel, J. Yin and N. Zheng, *Modulus-based iterative methods for constrained Tikhonov regularization*, J. Comput. Appl. Math., 2017, 319, 1–13.

[7] Z. Bai and D. J. Evans, *Matrix multisplitting relaxation methods for linear complementarity problems*, Int. J. Comput. Math., 1997, 63(3–4), 309–326.

[8] Z. Bai and D. J. Evans, *Matrix multisplitting methods with applications to linear complementarity problems: Parallel asynchronous methods*, Int. J. Comput. Math., 2002, 79(2), 205–232.

[9] Z. Bai, G. H. Golub and M. K. Ng, *Hermitian and skew-Hermitian splitting methods for non-Hermitian positive definite linear systems*, SIAM J. Matrix Anal. Appl., 2003, 24(3), 603–626.

[10] A. G. Bell, *On the production and reproduction of sound by light*, Am. J. Sci., 1880, 118(3), 305–324.

[11] X. L. Dean-Ben, A. Buehler and V. Ntziachristos, *Accurate model-based reconstruction algorithm for three-dimensional optoacoustic tomography*, IEEE Trans. Med. Imaging, 2012, 31(10), 1922–1928.

[12] X. L. Dean-Ben, V. Ntziachristos and D. Razansky, *Acceleration of optoacoustic model-based reconstruction using angular image discretization*, IEEE Trans. Med. Imaging, 2012, 31(5), 1154–1162.

[13] W. M. G. van Bokhoven, *Piecewise Linear Modeling and Analysis*, Proefschrift, Eindhoven, 1981.

[14] A. Buccini, M. Pasha and L. Reichel, *Modulus-based iterative methods for constrained $l_p - l_q$ minimization*, Inverse Probl., 2020, 36(8), 084001.

[15] R. W. Cottle, J. Pang and R. E Stone, *The Linear Complementarity Problem*, Academic Press, San Diego, 1992.

[16] C. W. Cryer, *The solution of a quadratic programming problem using systematic overrelaxation*, SIAM J. Control Optim., 1971, 9(3), 385–392.

[17] L. Ding, X. L. Dean-Ben and C. Lutzweiler, *Efficient non-negative constrained model-based inversion in optoacoustic tomography*, Phys. Med. Biol., 2015, 60(17), 6733.

[18] L. Ding, X. L. Dean-Ben and D. Razansky, *Real-time model-based inversion in cross-sectional optoacoustic tomography*, IEEE Trans. Med. Imaging, 2016, 35(8), 1883–1891.

[19] J. Dong, J. Gao, F. Ju and J. Shen, *Modulus methods for nonnegatively constrained image restoration*, SIAM J. Imaging Sci., 2016, 9(3), 1226–1246.

[20] J. Dong and M. Jiang, *A modified modulus method for symmetric positive-definite linear complementarity problems*, Numer. Linear Algebra Appl., 2009, 16(2), 129–143.

[21] Y. Dong, T. Görner and S. Kunis, *An algorithm for total variation regularized photoacoustic imaging*, Adv. Comput. Math., 2015, 41, 423–438.

[22] Y. Gao, W. Xu, Y. Chen, W. Xie and Q. Cheng, *Deep learning-based photoacoustic imaging of vascular network through thick porous media*, IEEE Trans. Med. Imaging, 2022, 41(8), 2191–2204.

[23] S. Gutta, S. K. Kalva, M. Pramanik and P. K. Yalavarthy, *Accelerated image reconstruction using extrapolated Tikhonov filtering for photoacoustic tomography*, Med. Phys., 2018, 45(8), 3749–3767.

[24] Y. Han, L. Ding and X. L. Dean-Ben, *Three-dimensional optoacoustic reconstruction using fast sparse representation*, Opt. Lett., 2017, 42(5), 979–982.

[25] Y. Hristova, P. Kuchment and L. Nguyen, *Reconstruction and time reversal in thermoacoustic tomography in acoustically homogeneous and inhomogeneous media*, Inverse Probl., 2008, 24(5), 055006.

[26] K. T. Hsu, S. Guan and P. V. Chitnis, *Fast iterative reconstruction for photoacoustic tomography using learned physical model: Theoretical validation*, Photoacoustics, 2023, 29, 100452.

[27] M. J. John and I. Barhumi, *Fast and efficient PAT image reconstruction algorithms: A comparative performance analysis*, Signal Processing, 2022, 201, 108691.

[28] R. A. Kruger, P. Liu and Y. Fang, *Photoacoustic ultrasound (PAUS)-reconstruction tomography*, Med. Phys., 1995, 2(10), 1605–1609.

[29] L. A. Kunyansky, *Explicit inversion formulae for the spherical mean Radon transform*, Inverse Probl., 2007, 23(1), 373.

[30] X. Li, L. Qi and S. Zhang, *Model-based optoacoustic tomography image reconstruction with non-local and sparsity regularizations*, IEEE Access, 2019, 7, 102136–102148.

[31] Y. Lou, W. Zhou and T. P. Matthews, *Generation of anatomically realistic numerical phantoms for photoacoustic and ultrasonic breast imaging*, J. Biomed. Opt., 2017, 22(4), 041015.

[32] O. L. Mangasarian, *Solutions of symmetric linear complementarity problems by iterative methods*, J. Optim. Theory Appl., 1977, 22(4), 465–485.

[33] K. G. Murty and F. Yu, *Linear Complementarity, Linear and Nonlinear Programming*, Heldermann-Verlag, Berlin, 1988.

[34] S. Na and L. V. Wang, *Photoacoustic computed tomography for functional human brain imaging*, Biomed. Opt. Express, 2021, 12(7), 4056–4083.

[35] B. Pan, S. R. Arridge and F. Lucka, *Photoacoustic reconstruction using sparsity in curvelet frame: Image versus data domain*, IEEE Trans. Comput. Imaging, 2021, 7, 879–893.

[36] J. Prakash, S. Mandal and D. Razansky, *Maximum entropy based non-negative optoacoustic tomographic image reconstruction*, IEEE Trans. Biomed. Eng., 2019, 66(9), 2604–2616.

[37] R. Prakash, D. Badal, A. Paul, D. Sonker and R. K. Saha, *Photoacoustic signal simulation using discrete particle approach and its application in tomography*, IEEE Trans. Ultrason. Ferroelectr. Freq. Control, 2020, 68(3), 707–717.

[38] C. B. Shaw, J. Prakash and M. Pramanik, *Least squares QR-based decomposition provides an efficient way of computing optimal regularization parameter in photoacoustic tomography*, J. Biomed. Opt., 2013, 18(8), 080501.

[39] K. Sivasubramanian, V. Periyasamy and M. Pramanik, *Non-invasive sentinel lymph node mapping and needle guidance using clinical handheld photoacoustic imaging system in small animal*, J. Biophotonics, 2018, 11(1), e201700061.

[40] B. Stephanian, M. T. Graham and H. Hou, *Additive noise models for photoacoustic spatial coherence theory*, Biomed. Opt. Express, 2018, 9(11), 5566–5582.

[41] Q. Huynh-Thu and M. Ghanbari, *Scope of validity of PSNR in image/video quality assessment*, Electron. Lett., 2008, 44(13), 800–801.

[42] B. E. Treeby and B. T. Cox, *k-Wave: MATLAB toolbox for the simulation and reconstruction of photoacoustic wave fields*, J. Biomed. Opt., 2010, 15(2), 021314.

[43] P. Tseng, *On linear convergence of iterative methods for the variational inequality problem*, J. Comput. Appl. Math., 1995, 60(1–2), 237–252.

[44] T. Wang, M. He, K. Shen, W. Liu and C. Tian, *Learned regularization for image reconstruction in sparse-view photoacoustic tomography*, Biomed. Opt. Express, 2022, 13(11), 5721–5737.

[45] Z. Wang, A. C. Bovik, H. R. Sheikh and E. P. Simoncelli, *Image quality assessment: From error visibility to structural similarity*, IEEE Trans. Image Process., 2004, 13(4), 600–612.

[46] Z. Wang, Z. Han and R. Hu, *Noise robust face hallucination employing Gaussian-Laplacian mixture model*, Neurocomputing, 2014, 133, 153–160.

[47] Z. Wang, H. Wang and S. Ren, *Research on ADMM reconstruction algorithm of photoacoustic tomography with limited sampling data*, IEEE Access, 2021, 9, 113631–113641.

[48] M. Xu and L. V. Wang, *Time-domain reconstruction for thermoacoustic tomography in a spherical geometry*, IEEE Trans. Med. Imaging, 2002, 21(7), 814–822.

[49] M. Xu and L. V. Wang, *Universal back-projection algorithm for photoacoustic computed tomography*, Phys. Rev. E., 2005, 71(1), 016706.

[50] M. Xu and L. V. Wang, *Photoacoustic imaging in biomedicine*, Rev. Sci. Instrum., 2006, 77(4), 041101.

[51] M. Xu, Y. Xu and L. V. Wang, *Time-domain reconstruction algorithms and numerical simulations for thermoacoustic tomography in various geometries*, IEEE Trans. Biomed. Eng., 2003, 50(9), 1086–1099.

[52] Y. Xu, D. Feng and L. V. Wang, *Exact frequency-domain reconstruction for thermoacoustic tomography, I. Planar geometry*, IEEE Trans. Med. Imaging, 2002, 21(7), 823–828.

[53] Y. Xu and L. V. Wang, *Time reversal and its application to tomography with diffracting sources*, Phys. Rev. Lett., 2004, 92(3), 033902.

[54] Y. Xu, M. Xu and L. V. Wang, *Exact frequency-domain reconstruction for thermoacoustic tomography, II. Cylindrical geometry*, IEEE Trans. Med. Imaging, 2002, 21(7), 829–833.

[55] P. K. Yalavarthy, S. K. Kalva and M. Pramanik, *Non-local means improves total-variation constrained photoacoustic image reconstruction*, J. Biophotonics, 2021, 14(1), e202000191.

[56] I. Yamaga, N. Kawaguchi Sakita and Y. Asao, *Vascular branching point counts using photoacoustic imaging in the superficial layer of the breast: A potential biomarker for breast cancer*, Photoacoustics, 2018, 11, 6–13.

[57] X. Yang, Y. Huang and L. Sun, *A modulus iteration method for retinex problem*, Numer. Linear Algebra Appl., 2018, 25(6), e2207.

[58] J. Zhang and X. Zhang, *A modulus iteration method for non-negatively constrained TV image restoration*, Comput. Math. Appl., 2023, 148, 62–69.

[59] Y. Zhang, Y. Wang and C. Zhang, *Total variation based gradient descent algorithm for sparse-view photoacoustic image reconstruction*, Ultrasonics, 2012, 52(8), 1046–1055.

[60] N. Zheng, K. Hayami and J. Yin, *Modulus-type inner outer iterative methods for nonnegative constrained least squares problems*, SIAM J. Matrix Anal. Appl., 2016, 37(3), 1250–1278.

Received October 2024; Accepted April 2025; Available online April 2025.